Analytical Methods

ROYAL SOCIETY OF CHEMISTRY

MINIREVIEW

View Article Online
View Journal | View Issue

Cite this: *Anal. Methods*, 2023, **15**, 4811

Electroanalytical overview: the sensing of carbendazim

Robert D. Crapnell, Prashanth S. Adarakatti and Craig E. Banks *

Carbendazim is a broad-spectrum systemic fungicide that is used to control various fungal diseases in agriculture, horticulture, and forestry. Carbendazim is also used in post-harvest applications to prevent fungal growth on fruits and vegetables during storage and transportation. Carbendazim is regulated in many countries and banned in others, thus, there is a need for the sensing of carbendazim to ensure that high levels are avoided which can result in potential health risks. One approach is the use of electroanalytical sensors which present a rapid, but highly selective and sensitive output, whilst being economical and providing portable sensing platforms to support on-site analysis. In this minireview, we report on the electroanalytical sensing of carbendazim overviewing recent advances, helping to elucidate the electrochemical mechanism and provide conclusions and future perspectives of this field.

Received 24th June 2023
Accepted 7th September 2023

DOI: 10.1039/d3ay01053h

rsc.li/methods

1. Introduction to carbendazim

Carbendazim (methyl *N*-(1*H*-benzimidazol-2-yl)carbamate) is a broad-spectrum systemic fungicide that is used to control various fungal diseases in agriculture, horticulture, and forestry. Carbendazim is a degradation product of benomyl and thiophanate-methyl which are used in fungicides and it has a half-life of 3 days to 12 months.[1] It belongs to the benzimidazole group of fungicides which exhibit broad-spectrum activity against various fungal pathogens and are widely used in agricultural and horticultural practices for disease control. Carbendazim is regulated in terms of maximum residue limits (MRLs) in various food products to ensure consumer safety. MRLs are the maximum concentrations of pesticide residues legally allowed in, or on food products. These limits are established based on extensive research and risk assessments conducted by regulatory authorities. MRLs values vary between different countries, for example, for apples, the levels are reported to be 5, 3, and 0.2 mg kg^{-1} for China, Japan, EU/UK while carbendazim is banned within USA

Faculty of Science and Engineering, Manchester Metropolitan University, Chester Street, Manchester M1 5GD, UK. E-mail: c.banks@mmu.ac.uk; Tel: +44 (0) 1612471196

Robert D. Crapnell achieved both his MChem and PhD from the University of Hull, United Kingdom, respectively, in 2014 and 2018. He is currently a senior research associate at Manchester Metropolitan University, United Kingdom. His research is predominantly focused on fundamental electrochemistry, additive manufacturing, sustainability, bespoke filament production and electrochemical and thermal biosensor development.

Prashanth S. Adarakatti did his post-graduation from P. C. Jabin Science College, Hubballi, India. He completed his Doctorate degree in 2017 from Central College, Bangalore University, India. Then he started his post-doctoral studies at the Indian Institute of Science (IISc), Bengaluru, India. He started his career working as an Assistant Professor of Chemistry at SVM Arts, Science and Commerce College, ILKAL, affiliated to Rani Channamma University, Belagavi, Karnataka, India. Currently, he is working as a research associate at Manchester Metropolitan University, Manchester, UK under Prof. Craig E. Banks' supervision. His research focuses on the development of electrochemical sensors and electroanalysis of energy materials.

and Australia.[1] Carbendazim is classed as a highly dangerous pesticide by the World Health Organization and has possible carcinogenic effects on humans.[2] The negative effects of carbendazim to human health have stimulated the reduction of the MRLs, and subsequently the development of reliable and sensitive detection methods are required.[3]

The measurement of carbendazim has been reported using high-performance liquid chromatography (HPLC) with fluorescence,[4] gas chromatography-mass spectrometry (GC-MS),[5] liquid chromatography-mass spectrometry (LC-MS)[6] and enzyme-linked immunosorbent assays,[7] noting that it is important that the specific sensing method chosen depends on the sample type, required sensitivity, regulatory requirements, and available resources. Validated and accredited laboratories often employ these techniques for reliable and accurate measurement of carbendazim and other pesticide residues. Such approaches can be costly, time consuming, require pretreatment, and can exhibit poor selectivity and are subject to large inaccuracies when applied into real samples. One approach is the use of electroanalytical sensors, which can deliver highly selective and sensitive outputs without specialized operators yet are rapid and economical. In this minireview, we provide a summary of the use of electroanalytical sensors for the measurement of carbendazim.

2. Electroanalytical based sensors for carbendazim

Table 1 shows a diverse range of electrochemical sensors that have been developed for the measurement of carbendazim which exhibit linear ranges in a low concentration range and have been applied to the measurement of carbendazim within many different samples, such as fruits, vegetables, tea, rice, soil, honey, and various water samples, to name just a few. As can be seen within Table 1, we have grouped them based upon the electrode material used, where it can be observed that glassy carbon (GC) is a favourite substrate but also the use of carbon paste electrodes (CPE), boron-doped diamond (BDD), screen-printed carbon electrodes (SPCE), pencil electrodes and additive manufacturing (AM, 3D-printing) are reported. We have split our mini-review into the sensing of carbendazim and then the simultaneous detection of carbendazim with other analytes; we highlight the most interesting and promising reports.

Craig E. Banks holds a personal chair in chemistry and has published over 600 papers and works on next generation additive manufacturing electrochemical sensing platforms.

We first consider the electrochemical oxidation of carbendazim, where a few mechanisms have been proposed, for example the oxidation mechanism occurs *via* a two-proton and two-electron transfer process with many different scenarios are presented. One particular scenario involves a two-proton and two-electron transfer process that produces methyl carbamate and an unstable benzimidazole radical, which react completely to form a dimer. Furthermore, the resulting dimer can also be electrochemically reduced to give the corresponding alcohol.[8] As shown within Fig. 1A, the electrochemical oxidation of carbendazim has been performed using a GC electrode where a well-defined oxidation peak (O1) is observed at +0.8 V (*vs.* SCE), and when the potential is returned, two reduction peaks are observed at +0.5 V (R1) and +0.3 V (R2), which are lower in intensities.[9] During the second scan, a second oxidation peak appears at +0.3 V (O2), corresponding to the electrochemical oxidation of carbendazim. Also shown within Fig. 1B is the effect upon changing the pH which confirms that the electrochemical mechanism involves electrons and protons. In order to unambiguously determine the electrochemical mechanism of carbendazim researchers must use high-resolution accurate mass spectrometry coupled with the electrolysis of carbendazim.[9] As shown in Fig. 1C, the main chemical species are observed, where the most feasible approach is that the electrochemical oxidation occurs *via* hydroxylation (forming COP_4) *via* four electrons and four protons. This is backed up by the elegant work of Hernandez and co-workers who measured the number of electrons which were determined coulometrically at a controlled potential, with a global transfer of 4 electrons.[10,11] Thus, the overall mechanism involves four electrons and four protons which shows a typical adsorption-controlled electrochemical process.

From inspection of Table 1, as expected, there is a range of nanoparticles that have been evaluated towards the sensing of carbendazim, such as platinum-doped nickel–cobalt oxide,[12] selenium with palladium,[13] graphitic carbon nitride,[14] gold nanoparticles,[15–17] samarium molybdate,[18] titanium dioxide,[19] platinum,[12] ytterbium oxide,[20] neodymium oxide,[21] tin selenium[22] and gadolinium sesquisulfide,[23] to name just a few. Using nanoparticles have enhanced electron-conducting properties and increased the electrochemical area of electrodes, however, most reports never mentioned is the cost of implementing such sensors.[24] Table 1 also shows the use of carbon nanotubes (CNT), which are attractive due to their unique nanogeometry and are ideal templates to immobilize nanoparticles, allowing the construction of designed nanoarchitecture. They are also beneficial on their own, they provide intrinsic properties, which include, high surface area, unique physical properties and morphology, high electrical conductivity and depending on the availability of edge plane sites/defects, this can give rise to improved electroanalytical properties.[25–27] Using CNTs has been the basis of β-cyclodextrin (β-CD) functionalized carbon nanosheets@carbon nanotubes (CNS@CNT) for the sensing of carbendazim.[28] This sensor was fabricated through the use of ball-milling CNTs with sodium citrate for 2 h. The

Table 1 An overview of the sensors reported for the measurement of carbendazim[a]

Electrode material	Electrode modification	Electroanalytical technique	Dynamic range	Limit of detection	Real sample	Reference
GC	Sodium montmorillonite clay	DPV	0.955–95.5 μM	5 ng mL^{-1}	Soil and water	62
GC	Polypyrrole	SWV	5–500 ng mL^{-1}	5 ng mL^{-1}	Soil and water	63
GC	MWCNTs/polymeric methyl red film	LSV	0.2–10 μM	9.0 nM	NA	64
GC	$ZnFe_2O_4$/SWCNTs	DPV	0.5–100 μM	0.09 μM	Apple, tomato, leek, paddy and sea water	57
GC	Functionalized MWCNTs	DPV	0.5–2.6 μM	0.5 μM	Soil and water	65
GC	PC4-EDOT-COOH	DPV	0.02–10 μM	3.5 nM	Paddy water and commercial juice	66
GC	Cyclodextrin–graphene nanosheets	DPV	5 nM–0.4 μM	2 nM	Water	67
GC	SiO_2/MWCNTs	SWV	0.2–4.0 μM	0.056 μM	Orange juice	68
GC	MWCNTs	SWV	0.256–3.11 μM	0.054 μM	River water	69
GC	β-cyclodextrin functionalized carbon nanosheets@carbon nanotubes	DPV	0.03–30 μM	9.4 nM	Apple juice	28
GC	Fullerene/MWCNT/Nafion	SWV	20–350 nM	17 nM	Soil	70
GC	MWCNTs-COOH	DPV	0.3–20 μM	0.06 μM	Cabbage, cucumber and potato	71
GC	GO-MWCNTs	DPV	10 nM–4 μM	5 nM	Soil and tap water	72
GC	Nano-porous gold	DPV	3.0–120 μM	0.24 μM	Waste and sea water	59
GC	$WO_3 \cdot 0.33H_2O$ nanorods	SWV	0.025–10 μM	22 nM	Dam, pond, lake, RO and tap water and soil samples	73
GC	Nd_2O_3 functionalized carbon nanofibers	DPV	0.1–243 μM	4.3 nM	Cabbage, brinjal, carrot, soil, drinking, tap and pond water	21
GC	Fe-doped copper vanadate	DPV	0.01–83.1 μM	5 nM	Apple juice and soy milk	74
GC	Mung bean-derived porous carbon@chitosan	DPV	0.1–20 μM	20 nM	Apple and tomato juices	75
GC	N-CNHs/PEI-CNTs	DPV	15 nM–70 μM	4 nM	Tap and lake water	76
GC	$Ti_3C_2T_x$ (MXene)	DPV	50 nM–100 μM	10.3 nM	NA	37
GC	MXene@AgNCs/NH_2-MWCNTs	DPV	0.3 nM–10 μM	0.1 nM	Lettuces	38
GC	Reduced holey graphene	DPV	0.1–100 μM	13.14 nM	River water and apple	77
GC	GdO nanorods/GA	DPV	0.01–75 μM	3 nM	River, tap and pond water	78
GC	$[Cu(adp)(BIB)(H_2O)]_n$	DPV	0.1–10 μM	10 nM	Tap water	79
GC	Nitrogen-doped hollow carbon nanofibers	DPV	0.1–25 μM	0.053 μM	NA	80
GC	Au nanorods@ZIF-8	DPV	0.0020–2.5 μM	0.33 nM	Paddy water, paddy soil, cucumber, water, spinach, strawberry and milk	81
GC	Ytterbium oxide nanorod/carbon nanofiber	DPV	50 nM–3035 μM	6 nM	Carrot, radish, lake and pond water	20
GC	$SnSe_2$ grafted N-doped carbon	CV	0.002–139.38 μM	0.67 nM	Water and vegetable extracts	22
GCPE	Graphene nanosheets/amberlite resin	DPV	8.36 nM–4.13 μM	3.1 nM	Soil, banana, waste and ground water, human blood serum and urine	34
GC	Sm_2O_3/rGO	DPV	0.019–0.198; 0.29–421.3 μM	3 nM	Orange juice, river and lake water and vegetables extract	35
GC	Au@Pt/CNHs@RGO	DPV	0.05–50 μM	1.64 nM	Carrot and orange juice	82
GC	$LaVO_4$/h-BN	Amperometry	0.001–89 μM	0.5 nM	Water and food samples	83
GC	Ru–Asp–Arg–GQD	DPV	0.01–45 μM	0.004 μM	Strawberry	84
GC	Graphene oxide/graphitic carbon nitride	SWV	0.008–0.1 μM	0.002 μM	Dam, lake and tap water	85

Table 1 (*Contd.*)

Electrode material	Electrode modification	Electroanalytical technique	Dynamic range	Limit of detection	Real sample	Reference
GC	Ni-doping nanoporous carbon-graphene composite	DPV	0.04–10.0 μM	8.9 nM	Pond water and juice samples	86
GC	PtNi/3D-NPC	DPV	0.5–30 μM	0.04 μM	Peach juice and vegetable samples	87
GC	Phosphorus-doped helical carbon nanofibers	DPV	0.1–35 μM	0.038 μM	Orange juice	88
GC	$Ti_3C_2T_x$ (MXene) and electrochemically reduced GO	DPV	2.0 nM–10.0 μM	0.67 nM	Cucumber and orange juice	37
GC	ERNGO	DPV	0.02–4.45 μM	5 nM	*Dendrobium candidum* powder	36
GC	MXene/carbon nanohorns/β-cyclodextrin-metal–organic frameworks	DPV	3.0 nM–10.0 μM	1.0 nM	Tomato	39
GC	Ti_2C MXene/Au–Ag nanoshuttles	DPV	0.006–9.8 μM	0.002 μM	Tea and rice samples	40
GC	Ayous sawdust-CNT	DPV	0.1–2.0 μM	0.04 μM	Grefonsec complex 210WP	31
GC	In_2S_3 nanotubes	DPV	5–80 μM	0.75 μM	Orange juice	30
GC	MWCNT-COOH/black phosphorus	SWV	9.0–1000 nM	4.0 nM	Pear, lake and tap water	8
GC	GO	SWV	0.1–2.4 μM	13.8 nM	Soil and water samples	89
GC	NiCo-LDH	DPV	0.006–14.1 μM	0.001 μM	NA	90
GC	Cobalt diselenide	DPV	0.01–2.43 μM and 2.43–382.43 μM	1.69 nM	Tomatoes and river water	91
GC	MoS_2/MWCNT	DPV	0.04–100 μM	7.4 nM	Tea and rice samples	92
GC	MIP/$CdMoO_4$/g–C_3N_4–15	DPV	10 pM–1 nM	2.5 pM	Apple and orange juices	49
GC	Vat violet 2R dye	SWV	0.05–0.7 μM	1.7725 nM	Soil and water	93
GC	Nitrogen and sulfur-doped hollow Mo_2C/C spheres/MIP	CV	1 pM–8 nM	0.67 pM	Grapes, apple, tomatoes, egg plant and cucumber	46
GC	C-ZIF-67@Ni/MIP	CV	0.4 pM–1 nM	0.135 pM	Soil and water	45
BDD		SWV	4.95–69 μM	1.6 μM	Lemon juice samples	60
BDD		SWV	0.5–15.0 μM	0.12 μM	Natural water	61
BDD	β-CD-MWCNTs	SWV	0.672–11.2 μM	0.196 μM	River water	94
Paper/SPCE		DPV	0.5–10 μM	0.06 μM	Apple and cabbage	51
SPCE	$Gd_2(WO_4)_3$ nanoflakes	DPV	0.02–40 μM	0.005 μM	Soil and rice	95
SPCE gloves		DPV	0.1–1 μM	0.047 μM	Apple, cabbage and orange juice	50
SPCE		DPV	0.1–1 μM	60 nM	Red and white wine	58
SPCE	Aptamer/CNT	DPV	1.0–50.0 nM	4.35 nM	Tomato	96
SPCE	Mo_2C@NiMn-LDH	DPV	0.001–232.14 μM	0.2 nM	Water and vegetables	97
SPE	Pt-doped $NiCo_2O_4$ nanograss	DPV	0.03–140 μM	0.005 μM	Tomato samples	12
SPE	Biosynthesized Au	Amperometry	0.05–25 μM	0.0029 μM	Soil	16
SPCE	Samarium molybdate	DPV	0.01–22 μM	1.0 nM	Pond and river water	18
SPE	Biosynthesized Au	Amperometry	0.05–50 μM	0.01 μM	Vegetables	15
SPCE	MWCNT	SWV	40 nM–0.4 μM	14 nM	Orange juice	29
SPCE	Se-GCN	DPV	0.099–346.6 μM	0.006 μM	Orange juice and vegetables extract	14
Carbon fiber ultramicroelectrode		DPV	0.1–2 μM	2.6 μM	Soil	11
Porous carbon		SWV	0.010–1.0 μM	0.0061 μM	River water, lettuce, and soil samples	98

Table 1 (*Contd.*)

Electrode material	Electrode modification	Electroanalytical technique	Dynamic range	Limit of detection	Real sample	Reference
Graphite epoxy	HKUST-1@MIPs	DPV	0.01–50 μM	2 nM	Tangerine, tomato, apple and cucumber juices	48
CPE		DPV	14 nM–0.2 μM	5 nM	River water and orange juice	99
CPE	MWCNTs/Ca-ZnO	SWV	0.01–0.45 μM	4.68 nM	Soil and water	100
CPE	Zeolite	SWV	12.9–777.7 nM	1.5 nM	Soy and cow milk	101
CPE	MWCNTs/MIP	SWV	0.1–50 nM	0.02 nM	Agricultural, waste and tap water, urine and strawberries	47
CPE	2-Hydroxy ethylammonium acetate	DPV	0.009–0.476 μM	1.69 nM	Grapes	102
CPE	Tricresyl phosphate	DPV	0.5–10 μM	0.3 μM	River water	103
CPE	Silver nanoparticles modified fumed silica	DPV	50 nM–3 μM	0.9 nM	River water and tomato, orange and apple juice	104
CPE	TiO_2	SWV	0.01–0.3 μM	17 nM	Soil and water samples	19
CPE	Reduced graphene oxide	DPV	30–900 nM	2.3 nM	Orange juice, lettuce leaves, drinking and wastewater	33
Graphite pencil electrode	Pd NPs	SWV	0.20–1.6 μM	0.018 μM	River water, synthetic urine	13
Additively manufactured		SWV	0.5–40.0 μM	0.09 μM	Honey	52

[a] Key: GC: glassy carbon; SWV: square-wave voltammetry; Pd NPs: palladium nanoparticles; DPV: differential pulse voltammetry; SWCNTs: single walled carbon nanotubes; MWCNTs: multi-walled carbon nanotubes; SWV: square-wave voltammetry; PC4-EDOT-COOH: poly(3,4-ethylenedioxythiophene); GO: graphene oxide; SPCE: screen-printed carbon electrode; MIP: molecular imprinted polymer; HKUST-1: $[Cu_3(BTC)_2(H_2O)_3]_n$; CP: carbon paste; CNHs: carbon nanohorns; PEI: polyethyleneimine; GCPE: glassy carbon paste electrode; rGO: reduced graphene oxide; EIS: Electrochemical impedance spectroscopy; AP: 1-aminopyrene; ERNGO: electrochemically reduced nitrogen-doped graphene oxide; NGO: nitrogen doped graphene oxide; BIB: 1,4-bisimidazolebenzene; H_2adp: adipic acid; GA: graphene aerogel; GCN: graphitic carbon nitride; GCN: graphitic carbon nitride; LDH: layered double-hydroxide; Ru: ruthenium; Asp: aspartic acid; Arg: arginine; GQD: graphene quantum dots; NPC: nano porous carbon; CPE: carbon paste electrode.

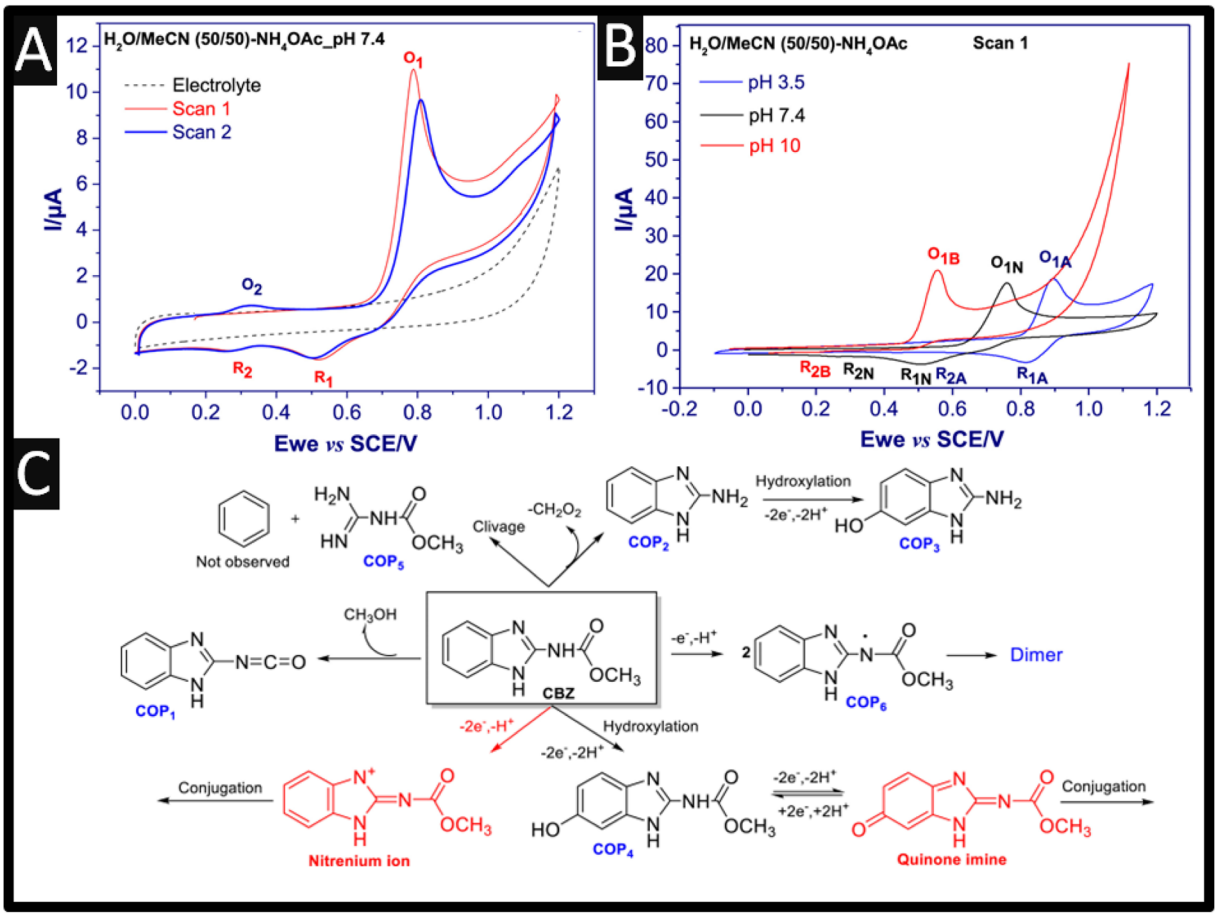

Fig. 1 (A) Cyclic voltammograms of 1 mM carbendazim in H_2O/MeCN 50 : 50 with 0.1 M ammonium acetate pH 7.4, scan rate 50 mV s^{-1}, and (B) cyclic voltammograms of 1 mM carbendazim at three different pH (Basic, B; Neutral, N and Acidic, A). (C) the main chemical species observed after the electrochemical oxidation of carbendazim. Figures reproducible from ref. 9. Copyright 2021 Elsevier.

composite was pyrolyzed at 850 °C for 3 h at a heating range of 3 °C min^{-1} under an argon atmosphere producing CNS@CNT; see Fig. 2A. Next, the CNS@CNT was mixed with β-CD within dimethyl formamide (DMF) under ultrasound, and then drop-cast upon a GC electrode. This sensor was able to measure carbendazim over the range of 0.03 to 30 µM with a limit of detection (LOD) reported to be 9.4 nM. The CNS@CNT combined large surface area of CNS and excellent electrical conductivity of CNT are responsible for their electroanalytical output along with β-CD possessing excellent host-guest supramolecular recognition ability, which could improve the selective recognition and enrichment capability toward carbendazim.[28] The sensor showed feasibility for the detection of carbendazim within spiked apple juice with recoveries of 97.1–99.4% reported. Other work has reported the use of a screen-printed carbon electrode modified with MWCNT and with the surfactant sodium dodecyl sulfate.[29] The surfactant increased the sensor's response to carbendazim, where the enhancement is attributed to the surfactants capacity to adsorb on a rough surface, such as carbon-based electrodes, *via* hydrophobic interactions to generate a surfactant-adsorbed layer. The higher peak currents observed results from a better adsorption and electrostatic interactions between carbendazim and this surfactant-adsorbed layer, which leads to an increase of carbendazim available at the electrode surface through the sodium dodecyl sulphate adsorbed layer.[29] This sensor provided a dynamic range of 40 nM to 0.4 µM with a LOD reported to be 14 nM. This sensor was validated through the measurement of carbendazim within spiked orange juice, which was compared to HPLC providing excellent recoveries. Work by Lan *et al.*[30] has reported on the use of In_2S_3 nanotubes, which involved taking a In salt with terephthalic acid *via* a solvothermal reaction within DMF at 100 °C for 30 min. This produced a metal–organic framework (MOF), MIL-68(In), which has an average length of 8–10 µm and a diameter of 500 nm. Next, the MIL-68(In) and thioacetamide were added to a methanol solution which was kept at 160 °C for 3 h forming In_2S_3 hollow nanotubes. This sensor exhibits a dynamic range of 5–80 µM, which was measured within orange juice. Of interest, fine particles of Ayous sawdust were successfully modified by maleic anhydride to increase their accumulation capability towards carbendazim, which were mixed with carbon nanotubes to yield a conductive composite.[31] This sensor was evaluated towards the detection of carbendazim within commercially available pesticide

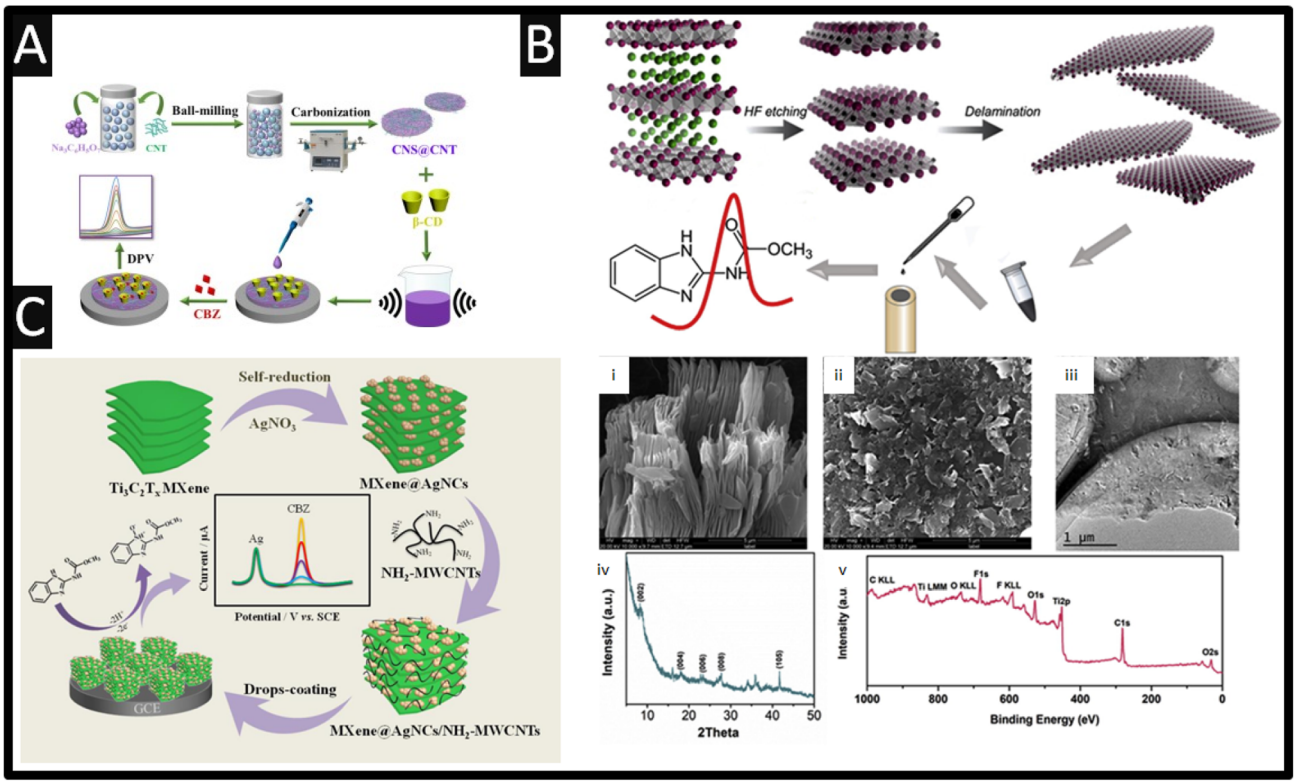

Fig. 2 (A) Fabrication of the of β-cyclodextrin (β-CD) functionalized carbon nanosheets@carbon nanotubes (CNS@CNT) sensor for the determination of carbendazim. Figure reproduced from ref. 28. Copyright 2022 Elsevier. (B) Scheme of carbendazim sensor preparation. SEM image (i) of etched $Ti_3C_2T_x$ and delaminated (ii) $Ti_3C_2T_x$. (iii) TEM image, (iv) XRD pattern and (v) XPS survey of $Ti_3C_2T_x$. Figure reproduced from ref. 37. Copyright 2019 Elsevier. (C) The synthetic route of MXene@AgNCs/NH_2-MWCNTs/GCE and its electrochemical application for the detection of carbendazim. Figure reproduced from ref. 38. Copyright 2021 Elsevier.

formulation (grefonsec complex 210WP, with carbendazim at 50 g per kg, as purchased from a local market) where a recovery of 90.3% was feasible.

Related to CNTs is graphene, which is akin to an unrolled nanotube. It is a single layer of atoms arranged in a hexagonal lattice nanostructure.[32] Pristine graphene is a poor electrochemical sensor because the majority of it comprises basal plane with a low amount of edge plane whereas, holey graphene, which has more assessable edge planes gives rise to improved electron transfer properties.[32] Reduced graphene oxide (GO) has been used for the sensing of carbendazim where the GO was made by the Hummers' method. This exfoliated graphite, which is then reduced to GO *via* treatment with ascorbic acid. The GO was then mixed with biochar, which was obtained through pyrolysis of *Eichhornia crassipes* biomass at 400 °C. This sensor exhibited a low dynamic range of 30–900 nM with an impressive LOD of 2.3 nM and was then successfully applied to the sensing of carbendazim within spiked orange juice, lettuce leaves, drinking and wastewater.[33] This has been extended to graphene nanosheets mixed with amberlite resin, which was shown to produce low nM ranges and was evaluated in spiked soil, banana, waste and ground water, blood serum and urine.[34] Further work has developed a nanoparticle (30–40 nm) Sm_2O_3/rGO composite, which was synthesised through a facile hydrothermal route.[35] This senor exhibits a dynamic range from 0.019–421.3 μM with a LOD of 3 nM and was evaluated toward the sensing of carbendazim within orange juice, river and lake water, and vegetable extract. Ya and co-workers[36] have reported on the electrochemically reduced nitrogen-doped graphene oxide-modified glassy carbon electrode. The nitrogen-doped graphene oxide was synthesised by taking graphite powder mixed with sulfuric acid and sodium nitrate, with potassium permanganate added into the mixture over 2 h. Next melamine was added in, which was stirred for 30 °C for 12 h. Last, hydrogen peroxide was added and the mixture was sonicated for 30 min and then washed. The electrochemical reduction was performed by drop-casting the nitrogen-doped graphene oxide onto a GC electrode, which was scanned using cyclic voltammetry from 0 to −1.0 V at a scan rate of 25 mV s^{-1} for 20 cycles. The sensor was able to measure carbendazim over the range 5.0–850 μg L^{-1} with a LOD of 1.0 μg L^{-1}. The author report that 5000-fold of sucrose, glucose, and fructose and a 1000-fold Na^+, K^+, Ca^{2+}, Mg^{2+}, Cu^{2+}, Zn^{2+}, Fe^{3+}, Al^{3+}, Cl^-, NO_3^-, CO_3^{2-}, and SO_4^{2-} and 200-fold methyl parathion, ethyl parathion, vitamin B1, B2, C, and E, L-aspartic acid, glutamic acid, serine, thiophanate, thiophanate-methyl, thiabendazole, endodsulfan, ametryn, fenamiphos, and benomyl did not interfere with the sensing of carbendazim. Furthermore, the authors reported that pesticides containing 200-fold of methyl parathion, ethyl parathion, thiophanate, thiophanate-methyl,

thiabendazole, endodsulfan, ametryn, fenamiphos, and benomyl did not affect the signal of carbendazim.[36] This sensor was evaluated with the sensing of carbendazim within spiked *Dendrobium candidum* powder with recoveries of 90.5–94.8%. The benefits of this sensor are reported to be a large electroactive area and its good conductivity.[36]

Transition metal carbides and nitrides (MXenes) are a family of two-dimensional materials originated from the selective etching "A" layer element of MAX phases, where M generally represents an early transition metal (*e.g.*, V, Nb, Ti, Mo), A stands for an A group element (Al or Si), and X refers to either carbon or nitrogen. MXenes are unique in that they possess a layered structure, consisting of transition metal carbide or nitride layers interleaved with functional groups, such as hydroxyl or other surface terminations. The versatility of MXenes arises from their tuneable properties, achieved by varying the transition metal, surface terminations, and layer thickness. This allows the researcher to tailor MXenes for specific applications by modifying their composition and structure. MXenes have properties such as high electrical conductivity, large specific surface areas, and notable electrochemical properties, thus MXenes have gained attention in the use of a carbendazim electroanalytical sensor. As shown within Fig. 2B, the overview of how $Ti_3C_2T_x$ MXene was prepared.[37] In summary, Ti_3AlC_2 is immersed into HF for 5 h providing etching, where after delamination was performed by sonication. Fig. 2B presents the SEM images of the etched, delaminated $Ti_3C_2T_x$ MXene along with a TEM image showing that the sample has a perfect layered structure.[37] X-ray diffraction (XRD) and X-ray photoelectron spectroscopy (XPS) are also shown (Fig. 2B), where the XRD pattern shows the characteristic (0 0 2) peak of the $Ti_3C_2T_x$ (8.3°), which was shifted from 9.5° in Ti_3AlC_2, suggesting that the etching process expanded the *d*-spacing between layers. The XPS survey shows signals from Ti, C, O and F elements showing the existence of F and O, which implied that the surface of the $Ti_3C_2T_x$ was terminated by –F and –O groups.[37] Using differential pulse voltammetry (DPV), the sensor was able to measure carbendazim over the range of 50 nM to 100 μM with a LOD reported to be 10.3 nM. The authors explored the 50-folds of common ions including Ca^{2+}, Na^{+}, Pb^{2+}, Zn^{2+}, NO_3^{-}, PO_4^{3-} and SO_4^{2-}, which showed no clear influence upon the sensing of carbendazim, while pesticides such as 10-folds of ametryn and fenamiphos also showed no clear influence. As shown within Fig. 2C, $Ti_3C_2T_x$ MXene can be self-reduced *via* the addition of silver nitrate producing MXene@Ag nanoclusters.[38] Next NH_2-MWCNT are mixed with the MXene@Ag nanoclusters within DMF and sonicated for 30 min to obtain MXene@AgNCs/NH_2-MWCNTs composites. This composite is then drop-cast onto a GC electrode which shows two peaks, one due to the electrochemical oxidation of silver, occurring at +0.12 V which can be used an internal reference and the second peak, +0.8 V, is due to the electrochemical oxidation of carbendazim. This sensor has a low LOD of 0.1 nM, and was shown to be successful in the measurement of carbendazim within lettuce samples with recoveries from 96.8 to 100.7% and RSD values less than 3.6%.[38] The other uses of MXenes have been developed for the sensing of

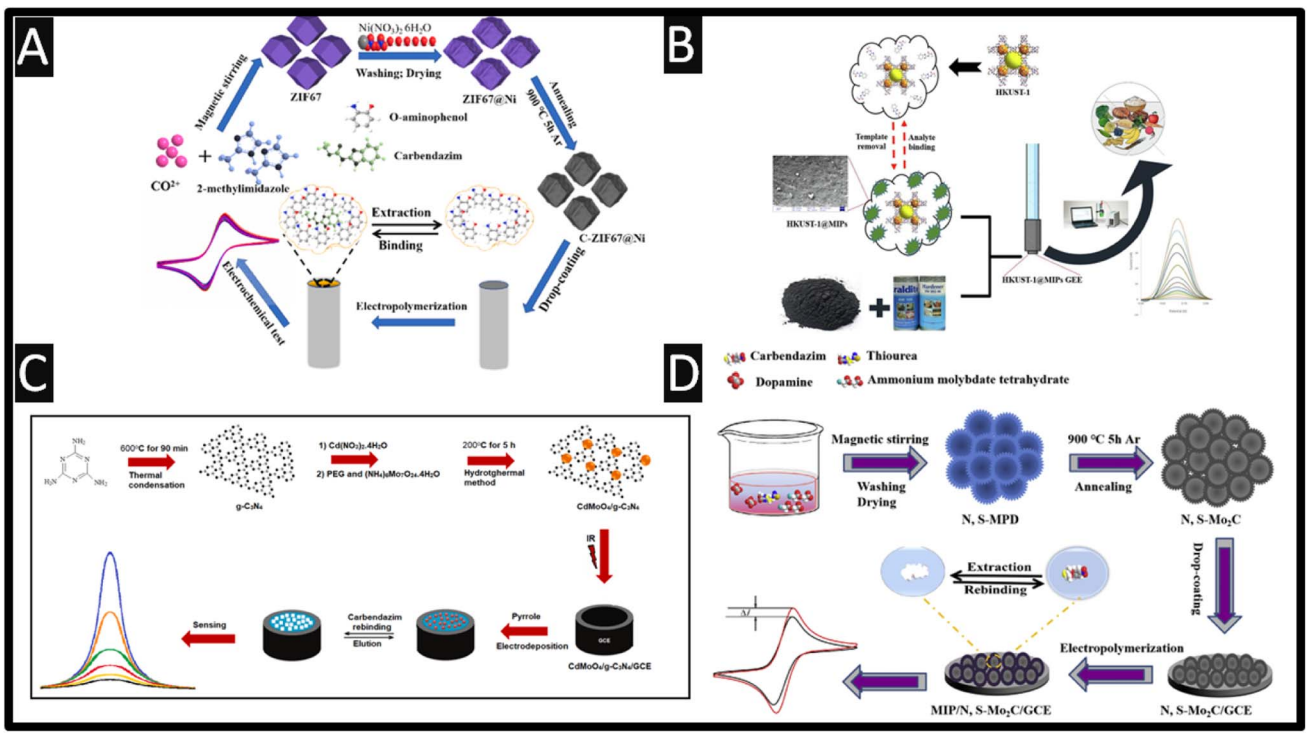

Fig. 3 (A) Schematic preparation process of MIP/C-ZIF67@Ni/GC; figure reproduced from ref. 45. Copyright 2022 Elsevier. (B) An overview of how a HKUST-1@MIP has been fabricated alongside DPV voltammetry. Figure reproduced from ref. 48. Copyright 2022 Elsevier. (C) Preparation protocol of $CdMoO_4$/g-C_3N_4 nanocomposite and CAR imprinted electrochemical electrode. Figure reproduced from ref. 49. Copyright 2022 Elsevier. (D) Schematic preparation process of carbendazim-MIP/N, S–Mo_2C/GC. Figure reproduced from ref. 46. Copyright 2019 Elsevier.

carbendazim within tomato,[39] cucumber and orange juice,[37] and tea and rice.[40]

Molecularly imprinted polymers (MIP) are bespoke synthetic recognition sites, designed for a specific target molecule and can have better, affinity and selectivity than their naturally occurring counterparts.[41–44] To this end, a variety of MIP sensors have been reported for the sensitive levels of carbendazim.[45–49] Fig. 3A shows how a C-ZIF67@Ni/MIP has been made for the detection of carbendazim from 0.4 pM to 1 nM with a LOD of 0.135 pM.[45] This was fabricated by taking cobalt and nickel salts with 2-methylimidazole dissolved into methanol and sonicating for 1 h. The product was centrifuged and washed, which was then placed into a vacuum furnace at 850 °C in an argon atmosphere at a heating rate of 5 °C min^{-1}. This C-ZIF67@Ni was drop cast upon a GC electrode and was then utilised for the formation of an electropolymerized MIP. Utilising *o*-aminophenol as the functional monomer with carbendazim as the target, the system was electrochemically polymerised by cyclic voltammetry through scanning at 50 mV s^{-1} from 0 to +0.8 V for 60 cycles. The template, carbendazim was removed by cyclic voltammetric scanning for 8 cycles within 0.1 M NaOH from −1.0 to +1.0 V until steady redox peaks were generated using a redox probe. This C-ZIF67@Ni/MIP sensor was explored within spiked soil and river water samples which have recoveries of 98.2–105.9% and 99.2–105.9%, respectively.

A graphite-epoxy electrode has been modified with MIP and a Cu-metal–organic framework.[48] The framework, $[Cu_3(BTC)_2(H_2O)_3]_n$ (HKUST-1) was synthesized *via* a solvothermal method. The MIP was formed *via* polymerisation by adding HKUST-1 with carbendazim and methacrylic acid dissolved within chloroform and was stirred for 60 min. Next ethylene glycol dimethyacrylate as cross-linker, and 2,2′-azobisisobutyronitrile as initiator were added and polymerization was initiated in an oil bath at 60 °C for 12 h with magnetic stirring. In order to remove the template molecules, a Soxhlet system with methanol : chloroform mixture (9 : 1 v/v) was used for 48 h. Finally, the HKUST-1@MIP was dried at 40 °C for one hour under vacuum and stored in a desiccator for further use.[48] This sensor displayed a dynamic range of 0.01 to 50 μM with a LOD of 2 nM, and was shown to measure carbendazim within spiked tangerine, tomato, apple and cucumber juices, which was validated against HPLC and showed that the HKUST-

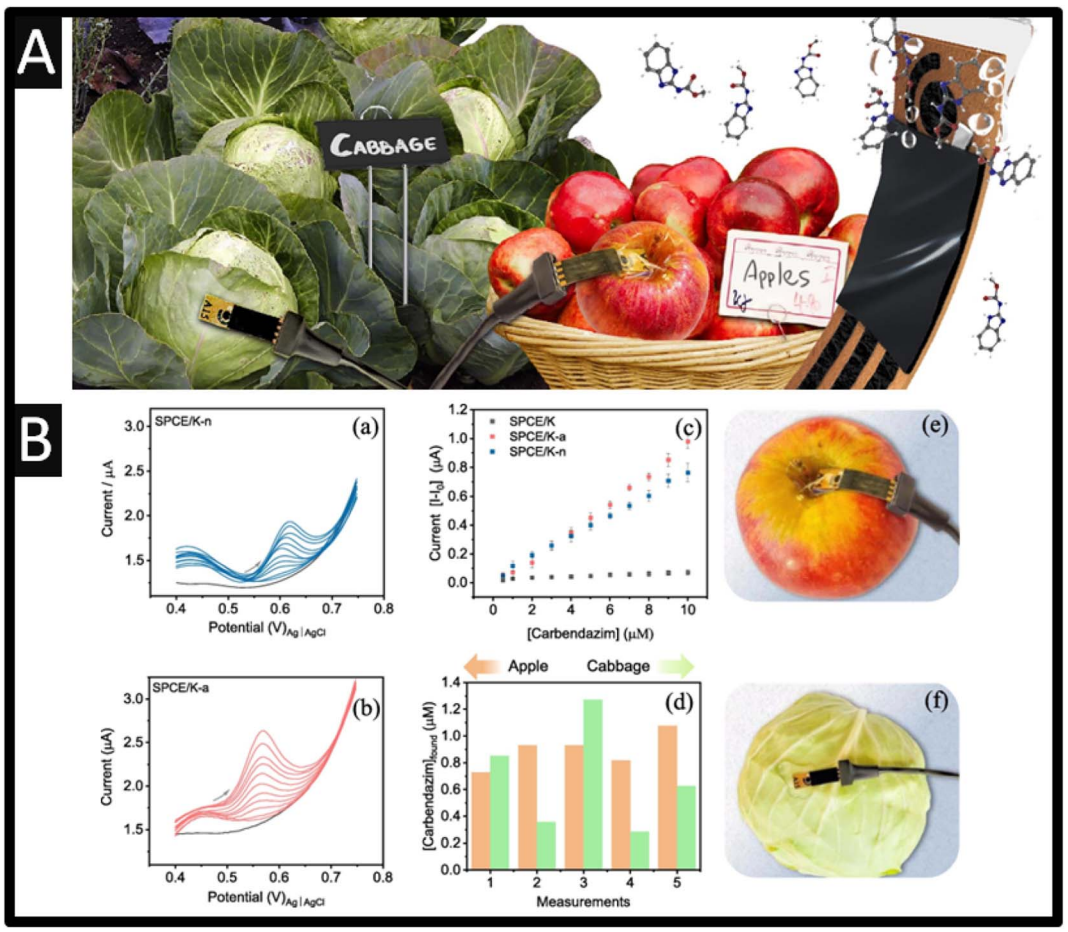

Fig. 4 (A) An overview of paper sensors allowed pesticide sensing on the skin of fruits and vegetables. (B) Differential pulse voltammograms for (a) SPCE/K-n and (b) SPCE/K-a at different concentrations of carbendazim (0.5, 1.0, 2.0, 3.0, 4.0, 5.0, 6.0, 7.0, 8.0, 9.0, 10 μM) and in the absence of carbendazim (grey line) in 0.1 M PB solution (pH 7.0). (c) Analytical curves for carbendazim on SPCE/K-n, SPCE/K-a, and SPCE/K. (d) Found concentrations of carbendazim on the surface of apple and cabbage with SPCE/K-a sensor. (e and f) Setup used in detecting carbendazim on apple and cabbage. Photos of the sensor and connector are also shown. Figures reproduced from ref. 51. Copyright 2023 Elsevier.

1@MIP sensor has practicability and effectiveness in the validation of real samples. Fig. 3C shows how a $CdMoO_4$/g-C_3N_4 nanocomposite is fabricated *via* one-pot *in situ* hydrothermal approach.[49] A MIP was produced *via* electrochemical polymerisation using pyrrole which was scanned for +0.3 to +1.2 V at a scan rate of 50 mV s^{-1}. This sensor exhibited a low dynamic range of 10 pM to 1 nM with a LOD of 2.5 pM; this was exemplified in the measurement of spiked carbendazim within apple and orange juices. Fig. 3D overviews the development of a sensor that utilises nitrogen and sulphur-doped hollow Mo_2C/C spheres (N, S-Mo_2C) and MIP for the sensing of carbendazim.[46] The fabrication of N, S-Mo_2C involved nitrogen and sulphur-doped molybdenum-polydopamine hollow spheres (N, S-MPD), which was synthesized and then carbonized in high temperature; see Fig. 4D for further details. The MIP was synthesised *via* electropolymerization using *o*-phenylenediamine as the functional monomer in the presence of carbendazim. The dynamic range of the sensor was from 1 pM to 8 nM with a LOD of 0.67 pM. Real sample analysis was performed of carbendazim in spiked fruits ($\sim 10^{-11}$M levels) and vegetables with the recoveries varying from 98.40 to 100.08% for grape, 95.45 to 97.74% for apple, 97.5 to 100.8% for tomatoes, 99.64 to 99.80% for eggplant and 95.20 to 98.19% for cucumber.

A novel approach is the use of sensors that can be applied directly to the measurement of carbendazim[50,51] avoiding the sample pre-treatment that is commonly required; see Fig. 4A. For example, Martins and co-workers have developed screen-printed carbon electrodes printed upon parchment (SPCE/P) and Kraft (SPCE/K) paper. Each electrode was electrochemically treated within acid (SPCE/P-a and SPCE/K-a) and with basic (SPCE/K-b and SPCE/P-b) or neutral medium (SPCE/K-n and SPCE/P-n), which involved cyclic voltammetry within the chosen medium from −2.5 V to +2.5 V five times. The authors reported that the Kraft paper gives rise to a larger electrode surface and with less resistance. As shown within Fig. 4B, the DPV is shown for SPCE/K-n and SPCE/K-a at different concentrations of carbendazim, which are compared to just SPCE/K where the SPCE/K-a. The provided a superior response due to the carboxylic groups formed during the activation; this sensor was able to detect carbendazim between 0.5 and 10 μM, with a detection limit of 0.06 μM. The authors demonstrated the sensing of carbendazim upon the surface of apple and cabbage, finding that concentrations found varied between 0.7 and 1.1

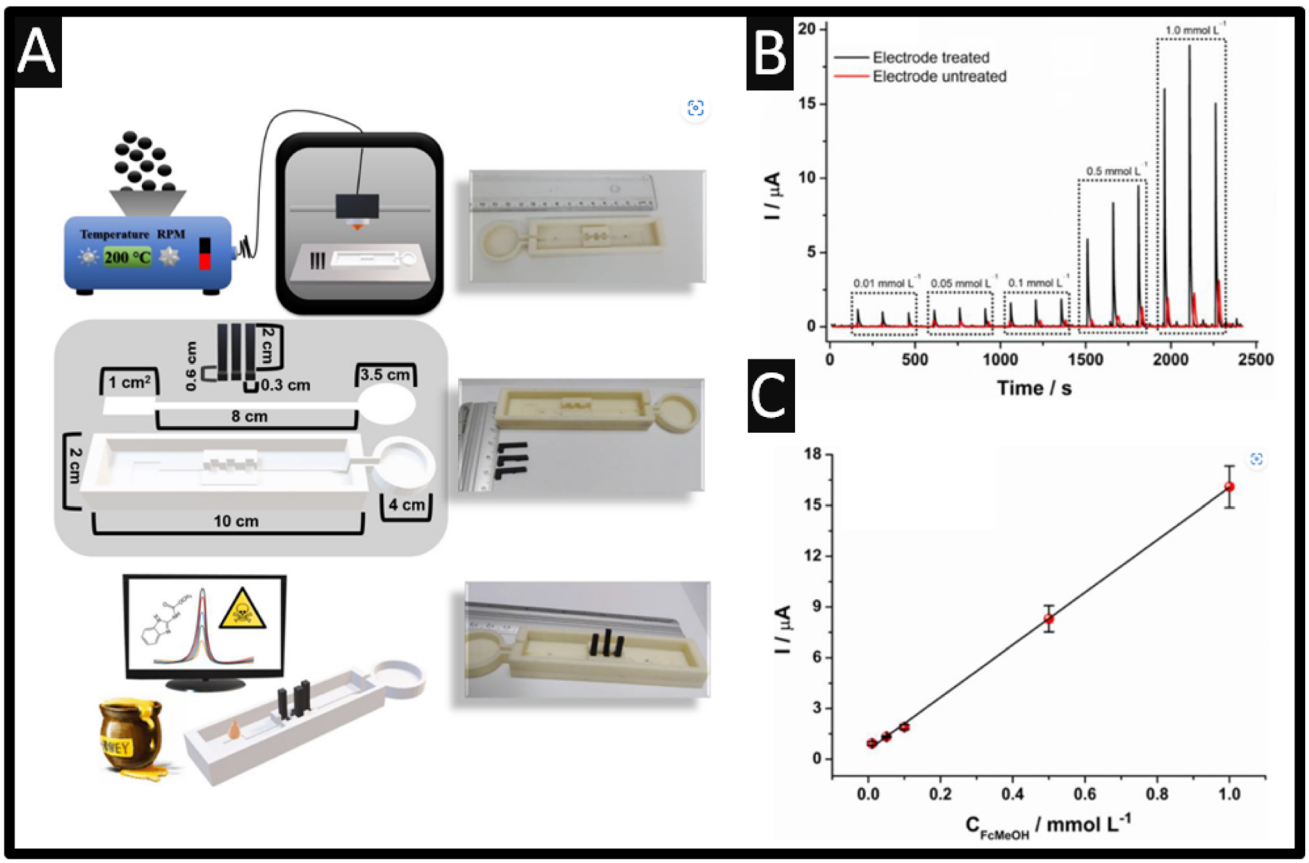

Fig. 5 (A) Illustration of a summary scheme of all the steps involved in this work. (top image) Production of conductive filaments with using a nanocarbon/PLA feedstocks, additive manufacturing of the microfluidic device based on non-conductive PLA filaments, and electrochemical sensors based on nanocarbon/PLA feedstocks, (middle image) structural scheme of the complete microfluidic device, sensors, fluidic paper, and base, with their respective dimensions. (bottom image) Analysis of carbendazim in honey from a portable potentiostat and microfluidic device using only a 30 μL drop. (B) Amperograms recorded for increasing concentrations of FcMeOH (0.01, 0.05, 0.1, 0.5, and 1.0 μM). Working potential: +0.1 V with the calibration plot (C). Reproduced from ref. 52. Copyright 2023 Elsevier.

μM for apples, and from 0.3 to 1.3 μM for cabbages. To investigate whether organic substances on the surface of the apple or cabbage could interfere with the detection of carbendazim, the reliability of the SPCE/K-a sensor was evaluated through recovery studies using a 0.1 M PB solution (pH 7) that had been exposed to apple or cabbage for 24 h[51] The values obtained were compared with those from the standard HPLC method where the recoveries with SPCE/K-a sensor ranged between 96 and 100.8% for apples and from 101.5 to 104.0% for cabbages, being equivalent to those from HPLC. This work shows a simple way to measure carbendazim in the skin of both types of samples, which is a demonstration of non-destructive, on-site monitoring of pesticides.[51]

Last, the use of additive manufactured (AM) sensors has been reported for the sensing of carbendazim.[52] The use of additive manufacturing allows one to provide low-cost, scalable, and the ability to obtain varied shapes and designs for fluidic platforms.[53] Recently, researchers have begun to design and produce their own conductive filament utilising different loadings and nanomaterials compared to the commercially available options.[54–56] Silva *et al.*[52] took this approach and have reported the design of a fully AM microfluidic platform coupled with a paper-based distribution channel for the sensing of carbendazim within in honey samples. As shown within Fig. 5A, a mixture of PLA and carbon black (28.5% wt) is extruded into a filament and fed into a 3D printer, which produces the conductive parts of the cell alongside a non-conductive PLA filament. These devices were printed on a rectangular mould with a width of 2 cm, a height of 10 cm, and a thickness of 1.5 cm, with the mould for the allocation of the filter paper responsible for the fluidic channel to the solution. In addition, the microfluidic system contained a mould for fitting the three electrodes, working, counter, and pseudo reference, so that they can be placed on the fluidic paper channel and a circular waste reservoir with a diameter of 3.5 cm at the end of the fluidic paper. As shown within Fig. 5B, the response of treated and untreated sensors is shown, where the best response is due to the treated sensor which is obtained by potential cycling within sodium hydroxide alongside the calibration plot (Fig. 6C) recorded within a pH 4 buffer. This sensor exhibited a dynamic range of 0.5–40 μM with a LOD of 0.09 μM. This sensor was evaluated within spiked wild and Jatai honey, which was diluted 1 : 1 with pH 4 buffer and exhibited 92.4–108.8% recoveries.[52]

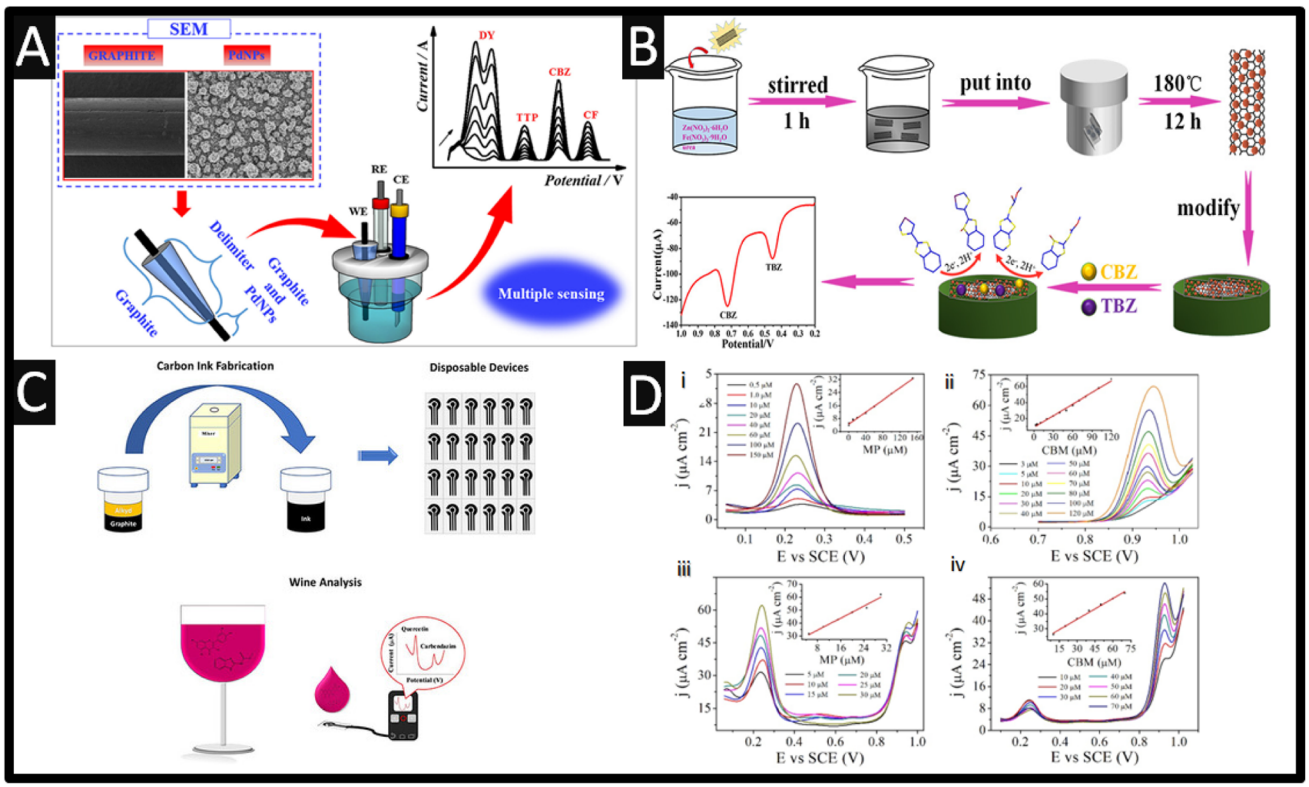

Fig. 6 (A) An overview of palladium nanoparticles supported upon a graphite pencil electrode direct to the sensing of direct yellow 50, tryptophan, carbendazim and caffeine. Figure reproduced from ref. 13. Copyright 2021 Elsevier. (B) An overview of the fabrication of $ZnFe_2O_4$/SWCNTs nanohybrid. Figure reproduced from ref. 57. Copyright 2017 American Chemical Society. (C) An overview of screen-printed electrodes are used for the simultaneous detection of quercetin and carbendazim. Figure reproduced from ref. 58. Copyright 2020 Wiley. (D) The detection of methyl parathion and carbendazim by the nano-porous gold electrode in HAC-NaAC solution (100 mM, pH 4.0). (i) The independent detection of methyl parathion within the range from 0.5 to 150 μM; (ii) the independent detection of carbendazim within the range from 3 to 120 μM; (iii) the selective detection of methyl parathionP in the presence of 20 μM carbendazim; (iv) the selective detection of carbendazim in the presence of 20 μM methyl parathion. The insert profiles show the calibration curves between the peak current density and the target pesticide concentration. Figure reproduced from ref. 59. Copyright 2019 Elsevier.

3. Electroanalytical based sensors for the simultaneous detection of carbendazim with other analytes

Wong and co-workers[13] reported the simultaneous detections of direct yellow 50, tryptophan, carbendazim, and caffeine in river water and synthetic urine samples using palladium nanoparticles (250–450 nm) supported upon a graphite pencil electrode (see Fig. 6A). All peaks are well resolved allowing them to be measured simultaneously given the underlying relevance and effects of the aforementioned substances, coupled with the fact that they are consumed and discarded in the environment.[13] The dynamic range for carbendazim was over the range 0.2–1.5 μM with a LOD reported to be 0.018 μM and was compared to a spectrophotometric method for all analytes.

The successful sensing of carbendazim and thiabendazole has been realized using a $ZnFe_2O_4$/SWCNTs nanohybrid (diameter ~100 nm).[57] As shown within Fig. 6B, the $ZnFe_2O_4$/SWCNTs nanohybrid was prepared *via* a facile one-step hydrothermal method, which involved iron and zinc salts with urea dissolved into ethanol where SWCNTs were added and stirred for 10 minutes. This was then poured into a Teflon-lined stainless-steel autoclave and was heated at 180 °C for 12 hours. After being washed, these were drop cast upon a GC electrode. The analytes are well-resolved, which benefited from the presence of CTAB, providing a dynamic range of 0.5–100.0 μM, with a LOD reported to be 0.09 μM. The author commented upon the signal enhancement: (i) there is a beneficial effect of dispersing $ZnFe_2O_4$ on SWCNTs and there are synergetic effects in the $ZnFe_2O_4$/SWCNTs composites, which are well dispersed on the surfaces of SWCNTs; (ii) the significant enhancements in the electrochemical response of carbendazim and thiabendazole could be ascribed to the large increase in the electroactive sites of the $ZnFe_2O_4$/SWCNTs electrode; (iii) $ZnFe_2O_4$/SWCNTs have excellent conductivity, which may be attributed to the strong synergistic effect between the $ZnFe_2O_4$ and SWCNTs, further accelerating the direct electron transfer.[57] The $ZnFe_2O_4$/SWCNTs nanohybrid sensor was successfully applied to the determination of CBZ and TBZ in the apple, tomato, leek, paddy and seawater.

As shown within Fig. 6C, screen-printed carbon electrodes were utilized to detect excessive concentrations of naturally occurring polyphenols and pesticide residues, namely the flavonoid quercetin and the pesticide carbendazim simultaneously in wine samples with a LOD of 60 nM reported for carbendazim.[58] The authors found that the use of an electrochemical pre-treatment through chronoamperometric experiments at a potential fixed of +1.2 V for 5 min in a saturated solution of sodium bicarbonate solution eliminated residues and impurities from the homemade carbon ink comprising graphite and alkyd resin eventually deposited on the electrodes.[58] The authors applied their sensor to the simultaneous detection of quercetin and carbendazim within white and red white observing 90–114% recoveries. Other notable work has been reported by Gao *et al.*,[59] namely the use of nano-porous gold deposited upon a GC electrode for the simultaneous sensing of methyl parathion and carbendazim which exhibited a large peak potential of +0.7 V between the two analytes. The nano-porous gold was prepared by chemical etching of Au/Ag binary alloy (50% Au, 50% Ag by weight) in concentrated nitric acid under free corrosion for 30 °C for 30 min. To remove residual nitric acid, the nano-porous gold was washed using ultrapure water until the pH of the ultrapure water was neutral. The treated nano-porous film was drop cast onto the surface of GC where Nafion® was then applied. This film possesses a nano-porous network structure with uniform pores ~35 nm in diameter and it has 100 nm thickness. The sensor measured 3.0 to 120 μM with a LOD reported to be 0.24 μM. for carbendazim. The authors explored the simultaneous detection of methyl parathion and carbendazim with interfering inorganic ions, both cations (Mg^{2+}, K^+, Na^+, and NH_4^+) and aqueous anions (SO_4^{2-}, PO_4^{3-}, CO_3^{2-}, and NO_3^-). The concentrations of these inorganic ions were 100 times higher than those of methyl parathion and carbendazim, and no interferences in the peak current densities of methyl parathion and carbendazim were noted, with the changes of peak current density were all below 3.51%. Additionally, the key interfering pesticides added were thiabendazole, methomyl, chlorpyrifos, tebuconazole, and benomyl, where their concentrations of the pesticides were two times higher than those of methyl parathion and carbendazim which didn't interfere. Last, the sensor was shown for the simultaneous detection of methyl parathion and carbendazim within spiked waste and seawater.

A useful approach is a development of screen-printing onto the fingers of rubber gloves that allows the sensing of carbendazim, diuron, paraquat and fenitrothion *via* simply touching with the finger onto apple, cabbage, and in orange juice.[50] As shown within Fig. 7A, three sensors are screen-printed onto three separate fingers, where one sensor is a pre-treated screen-printed carbon electrode while the other two are coated with carbon spherical shells (CSS) or with printed carbon nanoballs (PCNB).

The pre-treatment involved cyclic voltammetry within 0.5 M sulfuric acid between −2.5 to +2.5 V at a scan rate of 100 mV s^{-1} for two cycles. This approach was adopted since the simultaneous detection of carbendazim, diuron, paraquat, and fenitrothion using a single sensor was not suitable due to overlapping and poor definition of the oxidation peaks, and small current signals. Although, there is no data showing how the researchers connected the sensor to a potentiostat nor how to define the working electrode area. That said, as shown within Fig. 7A, the calibration plots are shown which were measured over the range of 0.1–1 μM with a LOD of 0.047 μM reported. As shown within Fig. 7B, the sensing was achieved on the skins of cabbages and apples where a drop of 500 μL of phosphate buffer solution (pH = 7) where a standard addition protocol was reported for the spiked value for carbendazim, diuron, paraquat and fenitrothion. The multidimensional projection technique least square projection again led to the highest discrimination capability of the pesticides with an average silhouette coefficient of 0.88 and the recoveries varied between 90 and 110%.[50] Such sensors are robust against flexion in multiple times and with their high selectivity, sensitivity, easy operation, and rapid pesticide detection, these glove-embedded sensors may also be employed in on-site analysis of other chemical threats and be extended to further environmental and

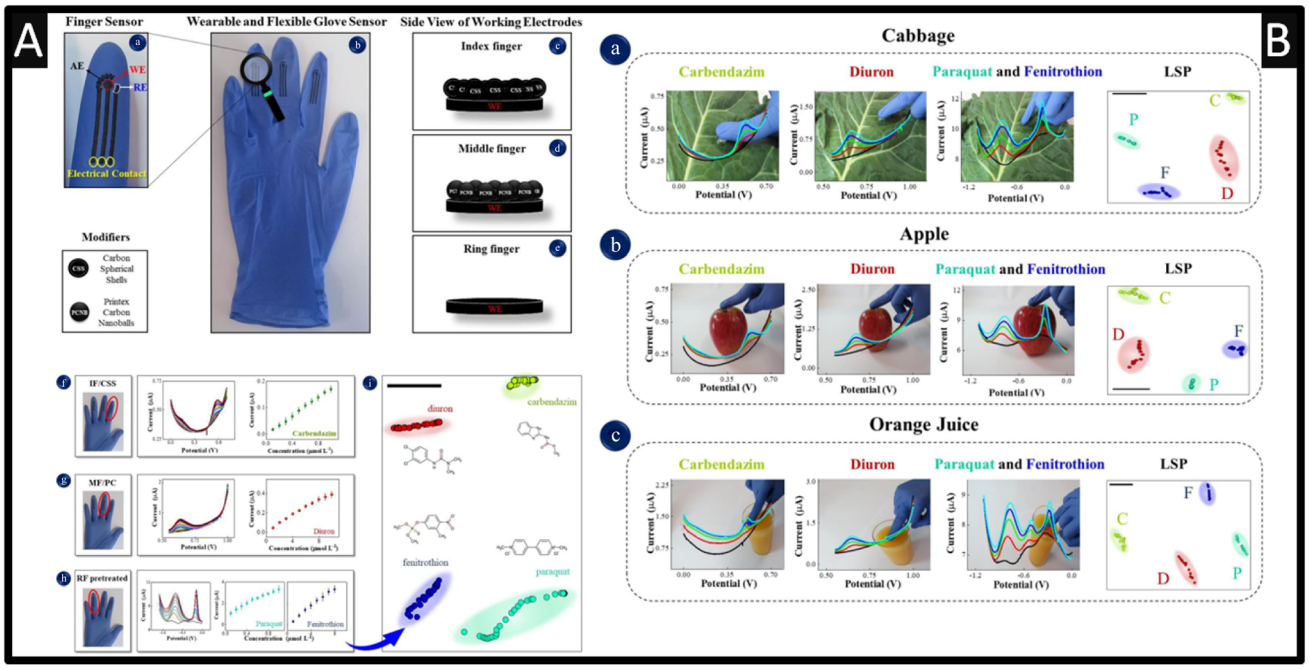

Fig. 7 (A): (a) Details of finger sensor design with a complete electrochemical system: auxiliary, reference and working electrodes. The connection between electrodes and potentiostat was made *via* flexible conductive wires for on-site detection. (b) Image of the real screen-printed sensing glove. (c–e) Schematic representation of the side views of CSS, PCNB and pre-treated sensing layers for index, middle and ring fingers, respectively. The electrochemical signatures and corresponding analytical curves obtained with index, middle and ring fingers of the glove-embedded sensors are shown in (f) through (h). (f) DP voltammograms for carbendazim detection from 0.1–1 μM; (g) DP voltammograms for diuron detection from 0.1–10 μM; (h) SW voltammograms for paraquat detection from 0.1–1 μM and fenitrothion detection from 0.1–10 μM. Conditions for detection: 0.1 M phosphate buffer solution, pH 7.0. (i) LSP plot for all pesticides measured with differential pulse and square wave voltammetry, where each voltammogram was converted into a coloured dot on the plot. The black bar is only a guide to measure distances between data points. The silhouette coefficient is 0.79. (B) Photos of actual measuring conditions with the wearable glove-embedded sensors on food samples of cabbage in (a), apple in (b) and orange juice in (c). Each photo is accompanied with the corresponding electrochemical screening of DPV signature and LSP plot for carbendazim and diuron made with IF/CSS and MF/PCNB, and SWV signature of paraquat and fenitrothion made with RF/pre-treated, also including the LSP plot. Figures reproduced from ref. 50. Copyright 2021 Elsevier.

water samples. Other work has reported the use of boron-doped diamond for the simultaneous sensing of carbendazim and fenamiphos, within lemon juice[60] and natural water.[61]

4. Conclusion and outlook

Carbendazim is a broad-spectrum systemic fungicide that is used to control various fungal diseases in agriculture, horticulture, and forestry. It is regulated in terms of maximum residue limits (MRLs) in various food products to ensure consumer safety. MRLs are the maximum concentrations of pesticide residues legally allowed in, or on food products. As such the development of electroanalytical sensing platforms is of interest. We collate the reports of the electroanalytical determination of carbendazim, categorising them in terms of the base electrode material, with the majority of reports utilising glassy carbon electrodes. Interesting works have been highlighted that use various electrode modifiers, including nanoparticles, MXenes and MIPs, while the use of MIPs are preferred as they provide selectivity when other analytes will be presented when detection carbendazim in real samples. The use of these electroanalytical systems has been shown to allow measurement of carbendazim, in some cases simultaneously with other analytes and applied *in situ* on food products. These systems must continue to be benchmarked against classical laboratory techniques to ensure confidence in the system and allow for products to penetrate the commercial market.

Author contributions

RDC: original draft, writing – review & editing. PSA: writing – review & editing; CEB: conceptualization, methodology, resources, formal analysis, writing – original draft, validation, writing – review & editing.

Conflicts of interest

There are no conflicts to declare.

References

1 S.-Y. Wang, X.-C. Shi, F.-Q. Liu and P. Laborda, *J. Agric. Food Chem.*, 2020, **68**, 11880–11894.
2 S. Singh, N. Singh, V. Kumar, S. Datta, A. B. Wani, D. Singh, K. Singh and J. Singh, *Environ. Chem. Lett.*, 2016, **14**, 317–329.

3 I. Suresh, S. Selvaraj, N. Nesakumar, J. B. B. Rayappan and A. J. Kulandaiswamy, *Trends Environ. Anal. Chem.*, 2021, **31**, e00137.
4 Q. Wu, Y. Li, C. Wang, Z. Liu, X. Zang, X. Zhou and Z. Wang, *Anal. Chim. Acta*, 2009, **638**, 139–145.
5 R. Paranthaman, A. Sudha and S. Kumaravel, *Am. J. Biochem. Biotechnol.*, 2012, **8**, 1–6.
6 H. S. Lee, M. M. Rahman, H. S. Chung, H. Kabir, K.-S. Yoon, S.-K. Cho, A. Abd El-Aty and J.-H. Shim, *J. Chromatogr. B*, 2018, **1095**, 1–7.
7 H. Liu, Y. Wang, R. Fu, J. Zhou, Y. Liu, Q. Zhao, J. Yao, Y. Cui, C. Wang and B. Jiao, *Anal. Methods*, 2021, **13**, 4256–4265.
8 X. Liao, X. Luo, Y. Li, Y. Zhou, Q. Liang, K. Feng, M. B. Camarada and J. Xiong, *Microchem. J.*, 2023, **190**, 108671.
9 R. C. T. Temgoua, U. Bussy, D. Alvarez-Dorta, N. Galland, J. Hémez, C. Thobie-Gautier, I. K. Tonlé and M. Boujtita, *Talanta*, 2021, **221**, 121448.
10 P. Hernandez, Y. Ballesteros, F. Galan and L. Hernandez, *Electroanalysis*, 1996, **8**, 941–946.
11 M. J. González de la Huebra, P. Hernández, O. Nieto, Y. Ballesteros and L. Hernández, *Fresenius. J. Anal. Chem.*, 2000, **367**, 474–478.
12 H. Mahmoudi-Moghaddam, H. Akbari Javar and Z. Garkani-Nejad, *Food Chem.*, 2022, **383**, 132398.
13 A. Wong, A. M. Santos, R. da Fonseca Alves, F. C. Vicentini, O. Fatibello-Filho and M. Del Pilar Taboada Sotomayor, *Talanta*, 2021, **222**, 121539.
14 N. Nataraj, T.-W. Chen, M. Akilarasan, S. M. Chen, A. A. Al-Ghamdi and M. S. Elshikh, *Chemosphere*, 2022, **302**, 134765.
15 W. Wang, F. Yao, D. Wang, X. Zhou, X. Wang, C. Zhao, M. Fang and J. Cai, *Int. J. Electrochem. Sci.*, 2017, **12**, 842–851.
16 L. Li and Z. Zhang, *Int. J. Electrochem. Sci.*, 2016, **11**, 4550–4559.
17 C. Zhu, D. Liu, Z. Chen, L. Li and T. You, *J. Colloid Interface Sci.*, 2019, **546**, 92–100.
18 T. Kokulnathan, E. Ashok Kumar and T.-J. Wang, *Microchem. J.*, 2020, **158**, 105227.
19 L. Killedar, D. Ilager, S. J. Malode and N. P. Shetti, *Mater. Chem. Phys.*, 2022, **285**, 126131.
20 A. Krishnapandi, S. M. Babulal, S.-M. Chen, S. Palanisamy, S.-C. Kim and M. Chiesa, *J. Environ. Chem. Eng.*, 2023, **11**, 109059.
21 S. Palanisamy, K. Alagumalai, M. Chiesa and S.-C. Kim, *Environ. Res.*, 2023, **219**, 115140.
22 P. Santhoshkumar, B. Thirumalraj, B. Sriram, K. Karuppasamy, D. Vikraman, A. Kathalingam, H. Choe and H.-S. Kim, *Ceram. Int.*, 2022, **48**, 16023–16032.
23 K. Y. Kumar, M. Prashanth, L. Parashuram, B. Palanivel, F. A. Alharti, B.-H. Jeon and M. Raghu, *Chemosphere*, 2022, **296**, 134030.
24 R. D. Crapnell and C. E. Banks, *Microchim. Acta*, 2021, **188**, 1–23.
25 X. Ji, R. O. Kadara, J. Krussma, Q. Chen and C. E. Banks, *Electroanalysis*, 2010, **22**, 7–19.
26 W. Wang, F. Lu, L. M. Veca, M. J. Meziani, X. Wang, L. Cao, L. Gu and Y.-P. Sun, in *Encyclopedia of Inorganic and Bioinorganic Chemistry*, 2012, DOI: **10.1002/9781119951438.eibc0320**.
27 C. Kalinke, R. D. Crapnell, E. Sigley, M. J. Whittingham, P. R. de Oliveira, L. C. Brazaca, B. C. Janegitz, J. A. Bonacin and C. E. Banks, *Chem. Eng. J.*, 2023, **467**, 143513.
28 R. Liu, B. Li, F. Li, V. Dubovyk, Y. Chang, D. Li, K. Ding, Q. Ran, G. Wang and H. Zhao, *Food Chem.*, 2022, **384**, 132573.
29 J. M. Petroni, B. G. Lucca, D. K. Fogliato and V. S. Ferreira, *Electroanalysis*, 2016, **28**, 1362–1369.
30 L. Lan, B. Li, X. Chen, Y. Gao and X. Kuang, *ChemNanoMat*, 2023, **9**, e202200522.
31 G. A. Fozing Mekeuo, C. Despas, C. Péguy Nanseu-Njiki, A. Walcarius and E. Ngameni, *Electroanalysis*, 2022, **34**, 667–676.
32 D. A. C. Brownson, D. K. Kampouris and C. E. Banks, *Chem. Soc. Rev.*, 2012, **41**, 6944–6976.
33 M. V. S. Sant'Anna, S. W. M. M. Carvalho, A. Gevaerd, J. O. S. Silva, E. Santos, I. S. C. Carregosa, A. Wisniewski, L. H. Marcolino-Junior, M. F. Bergamini and E. M. Sussuchi, *Talanta*, 2020, **220**, 121334.
34 N. G. Khare, R. A. Dar and A. K. Srivastava, *Electroanalysis*, 2015, **27**, 1915–1924.
35 T. Sakthi Priya, N. Nataraj, T.-W. Chen, S.-M. Chen and T. Kokulnathan, *Chemosphere*, 2022, **307**, 135711.
36 Y. Ya, C. Jiang, L. Mo, T. Li, L. Xie, J. He, L. Tang, D. Ning and F. Yan, *Food Anal. Methods*, 2017, **10**, 1479–1487.
37 D. Wu, M. Wu, J. Yang, H. Zhang, K. Xie, C.-T. Lin, A. Yu, J. Yu and L. Fu, *Mater. Lett.*, 2019, **236**, 412–415.
38 W. Zhong, F. Gao, J. Zou, S. Liu, M. Li, Y. Gao, Y. Yu, X. Wang and L. Lu, *Food Chem.*, 2021, **360**, 130006.
39 X. Tu, F. Gao, X. Ma, J. Zou, Y. Yu, M. Li, F. Qu, X. Huang and L. Lu, *J. Hazard. Mater.*, 2020, **396**, 122776.
40 X. Zhu, P. Liu, T. Xue, Y. Ge, S. Ai, Y. Sheng, R. Wu, L. Xu, K. Tang and Y. Wen, *Ceram. Int.*, 2021, **47**, 173–184.
41 O. Jamieson, F. Mecozzi, R. D. Crapnell, W. Battell, A. Hudson, K. Novakovic, A. Sachdeva, F. Canfarotta, C. Herdes, C. E. Banks, H. Snyder and M. Peeters, *Phys. Status Solidi A*, 2021, **218**, 2100021.
42 J. McClements, L. Bar, P. Singla, F. Canfarotta, A. Thomson, J. Czulak, R. E. Johnson, R. D. Crapnell, C. E. Banks, B. Payne, S. Seyedin, P. Losada-Pérez and M. Peeters, *ACS Sens.*, 2022, **7**, 1122–1131.
43 R.-N. Chen, S.-H. Kang, J. Li, L.-N. Lu, X.-P. Luo and L. Wu, *Anal. Methods*, 2021, **13**, 4538–4556.
44 R. D. Crapnell, N. C. Dempsey-Hibbert, M. Peeters, A. Tridente and C. E. Banks, *Talanta Open*, 2020, **2**, 100018.
45 Y. Li, X. Chen, H. Ren, X. Li, S. Chen and B.-C. Ye, *Talanta*, 2022, **237**, 122909.
46 S. Feng, Y. Li, R. Zhang and Y. Li, *Biosens. Bioelectron.*, 2019, **142**, 111491.
47 A. Kasaeinasab, H. A. Mahabadi, S. J. Shahtaheri, F. Faridbod, M. R. Ganjali and F. Mesgari, *PLoS One*, 2023, **18**, e0279816.

48 F. Beigmoradi, M. Rohani Moghadam, A. Bazmandegan-Shamili and H. R. Masoodi, *Microchem. J.*, 2022, **179**, 107633.
49 M. L. Yola, *Chemosphere*, 2022, **301**, 134766.
50 P. A. Raymundo-Pereira, N. O. Gomes, F. M. Shimizu, S. A. S. Machado and O. N. Oliveira, *Chem. Eng. J.*, 2021, **408**, 127279.
51 T. S. Martins, S. A. S. Machado, O. N. Oliveira and J. L. Bott-Neto, *Food Chem.*, 2023, **410**, 135429.
52 L. R. G. Silva, J. S. Stefano, R. D. Crapnell, C. E. Banks and B. C. Janegitz, *Talanta Open*, 2023, **7**, 100213.
53 M. J. Whittingham, R. D. Crapnell, E. J. Rothwell, N. J. Hurst and C. E. Banks, *Talanta Open*, 2021, **4**, 100051.
54 R. D. Crapnell, E. Sigley, R. J. Williams, T. Brine, A. Garcia-Miranda Ferrari, C. Kalinke, B. C. Janegitz, J. A. Bonacin and C. E. Banks, *ACS Sustain. Chem. Eng.*, 2023, **11**(24), 9183–9193.
55 E. Sigley, C. Kalinke, R. D. Crapnell, M. J. Whittingham, R. J. Williams, E. M. Keefe, B. C. Janegitz, J. A. Bonacin and C. E. Banks, *ACS Sustain. Chem. Eng.*, 2023, **11**, 2978–2988.
56 P. Wuamprakhon, R. D. Crapnell, E. Sigley, N. J. Hurst, R. J. Williams, M. Sawangphruk, E. M. Keefe and C. E. Banks, *Adv. Sustainable Syst.*, 2023, **7**, 2200407.
57 Y. Dong, L. Yang and L. Zhang, *J. Agric. Food Chem.*, 2017, **65**, 727–736.
58 P. A. Raymundo-Pereira, N. O. Gomes, J. H. S. Carvalho, S. A. S. Machado, O. N. Oliveira Jr and B. C. Janegitz, *ChemElectroChem*, 2020, **7**, 3074–3081.
59 X. Gao, Y. Gao, C. Bian, H. Ma and H. Liu, *Electrochim. Acta*, 2019, **310**, 78–85.
60 T. Lima, H. T. D. Silva, G. Labuto, F. R. Simões and L. Codognoto, *Electroanalysis*, 2016, **28**, 817–822.
61 R. F. França, H. P. M. de Oliveira, V. A. Pedrosa and L. Codognoto, *Diamond Relat. Mater.*, 2012, **27–28**, 54–59.
62 P. Manisankar, G. Selvanathan and C. Vedhi, *Appl. Clay Sci.*, 2005, **29**, 249–257.
63 P. Manisankar, G. Selvanathan and C. Vedhi, *Int. J. Environ. Anal. Chem.*, 2005, **85**, 409–422.
64 J. Li and Y. Chi, *Pestic. Biochem. Physiol.*, 2009, **93**, 101–104.
65 P. L. A. Sundari, S. P. Palaniappan and P. Manisankar, *Anal. Lett.*, 2010, **43**, 1457–1470.
66 Y. Yao, Y. Wen, L. Zhang, Z. Wang, H. Zhang and J. Xu, *Anal. Chim. Acta*, 2014, **831**, 38–49.
67 Y. Guo, S. Guo, J. Li, E. Wang and S. Dong, *Talanta*, 2011, **84**, 60–64.
68 C. A. Razzino, L. F. Sgobbi, T. C. Canevari, J. Cancino and S. A. S. Machado, *Food Chem.*, 2015, **170**, 360–365.
69 W. F. Ribeiro, T. M. G. Selva, I. C. Lopes, E. C. S. Coelho, S. G. Lemos, F. Caxico de Abreu, V. Bernardo do Nascimento and M. C. Ugulino de Araújo, *Anal. Methods*, 2011, **3**, 1202–1206.
70 D. N. Teadoum, S. K. Noumbo, K. T. Arnaud, T. T. Ranil, A. D. Mvondo Zé and I. K. Tonle, *Int. J. Electrochem.*, 2016, **2016**, 7839708.
71 L. Fang, W. Xinfa, V. I. Dubovyk and L. Runqiang, *Bulletin of Sumy National Agrarian University. The series: Agronomy and Biology*, 2022, **46**, 76–82.
72 S. Luo, Y. Wu and H. Gou, *Ionics*, 2013, **19**, 673–680.
73 D. Ilager, H. Seo, S. S. Kalanur, N. P. Shetti and T. M. Aminabhavi, *J. Environ. Manage.*, 2021, **279**, 111611.
74 A. Yamuna, T.-W. Chen, S.-M. Chen and T.-Y. Jiang, *Microchim. Acta*, 2021, **188**, 277.
75 R. Liu, Y. Chang, F. Li, V. Dubovyk, D. Li, Q. Ran and H. Zhao, *Food Chem.*, 2022, **392**, 133301.
76 X. Chen, W. Li, C. Lu, J. Chu, R. Lin, P. Wang, G. Xie, Q. Gu, D. Wu and B. Chu, *Sci. Total Environ.*, 2022, **851**, 158324.
77 Y. Yang, Z. Chen, Q. Wang, Q. Wang and Y. Zhang, *Phys. Status Solidi A*, 2022, **219**, 2100412.
78 T. Kokulnathan and S.-M. Chen, *ACS Appl. Mater. Interfaces*, 2020, **12**, 16216–16226.
79 Y.-w. Hu, W. Wang, H.-e. Li, Q.-k. Li and K.-k. Niu, *Int. J. Electrochem. Sci.*, 2018, **13**, 5031–5040.
80 P. Yang, X. Pan, J. Wang, R. Yang, J. Chu, H. Chen, H. Nan, L. Yang and X. Zhao, *ChemistrySelect*, 2019, **4**, 2059–2063.
81 T. Gan, J. Li, H. Li, Y. Liu and Z. Xu, *Nanoscale*, 2019, **11**, 7839–7849.
82 W. Li, P. Wang, B. Chu, X. Chen, Z. Peng, J. Chu, R. Lin, Q. Gu, J. Lu and D. Wu, *Food Chem.*, 2023, **402**, 134197.
83 B. Sriram, J. N. Baby, Y.-F. Hsu, S.-F. Wang and M. George, *Inorg. Chem.*, 2021, **60**, 5271–5281.
84 D. Xu, R. Li, G. Wang, H. Zhu and Z. Li, *New J. Chem.*, 2021, **45**, 21308–21314.
85 D. Ilager, N. P. Shetti, Y. Foucaud, M. Badawi and T. M. Aminabhavi, *Chemosphere*, 2022, **292**, 133450.
86 L. Guo, B. Zhao, L. Hao, Y. Zhang and C. Wang, *Microchim. Acta*, 2022, **189**, 454.
87 L. Yang, Y.-P. Zhu, A.-J. Wang, X. Weng and J.-J. Feng, *Microchim. Acta*, 2023, **190**, 211.
88 R. Cui, D. Xu, X. Xie, Y. Yi, Y. Quan, M. Zhou, J. Gong, Z. Han and G. Zhang, *Food Chem.*, 2017, **221**, 457–463.
89 D. Ilager, S. J. Malode and N. P. Shetti, *Chemosphere*, 2022, **303**, 134919.
90 T. Kokulnathan, T.-J. Wang, F. Ahmed and N. Arshi, *Surf. Interfaces*, 2023, **36**, 102570.
91 E. Tamilalagan, M. Akilarasan, S.-M. Chen, S. Maheshwaran and Y.-F. Huang, *Colloids Surf., A*, 2022, **653**, 129941.
92 X. Zhu, P. Liu, Y. Ge, R. Wu, T. Xue, Y. Sheng, S. Ai, K. Tang and Y. Wen, *J. Electroanal. Chem.*, 2020, **862**, 113940.
93 N. P. Shetti, K. Prabhu and S. J. Malode, *Electrochemical Detection and Degradation of Carbendazim at Poly (Vat Violet 2r) Modified GCE*, 2021, available at SSRN 3928374.
94 M. Brycht, O. Vajdle, K. Sipa, J. Robak, K. Rudnicki, J. Piechocka, A. Tasić, S. Skrzypek and V. Guzsvány, *Ionics*, 2018, **24**, 923–934.
95 S. Periyasamy, J. Vinoth Kumar, S.-M. Chen, Y. Annamalai, R. Karthik and N. Erumaipatty Rajagounder, *ACS Appl. Mater. Interfaces*, 2019, **11**, 37172–37183.
96 C. J. Venegas, L. Rodríguez and P. Sierra-Rosales, *Chemosensors*, 2023, **11**, 117.
97 X. B. Joseph, J. N. Baby, S.-F. Wang, B. Sriram and M. George, *ACS Sustain. Chem. Eng.*, 2021, **9**, 14900–14910.
98 L. Wei, X. Huang, J. Yang, Y. Wang, K. Huang, L. Xie, F. Yan, L. Luo, C. Jiang, J. Liang, T. Li and Y. Ya, *J. Electroanal. Chem.*, 2022, **915**, 116370.

99 G. J. Arruda, F. D. Lima and C. A. L. Cardoso, *J. Environ. Sci. Health, Part B*, 2016, **51**, 534–539.
100 S. J. Malode, P. K. Keerthi, N. P. Shetti and R. M. Kulkarni, *Electroanalysis*, 2020, **32**, 1590–1599.
101 E. M. Maximiano, F. de Lima, C. A. L. Cardoso and G. J. Arruda, *J. Appl. Electrochem.*, 2016, **46**, 713–723.
102 J. F. de Macedo, A. A. C. Alves, M. V. S. Sant'Anna, F. G. C. Cunha, G. d. A. R. Oliveira, L. M. Lião and E. M. Sussuchi, *J. Appl. Electrochem.*, 2022, **52**, 729–742.
103 A. M. Ashrafi, J. Đorđević, V. Guzsvany, I. Švancara, T. Trtić-Petrović, M. Purenović and K. Vytřas, *Int. J. Electrochem. Sci.*, 2012, **7**, 9717–9731.
104 A. Özcan, F. Hamid and A. A. Özcan, *Talanta*, 2021, **222**, 121591.

